THE JOURNAL OF PHYSICAL CHEMISTRY C
A JOURNAL OF THE AMERICAN CHEMICAL SOCIETY

pubs.acs.org/JPCC

Article

Combined NMR and Isothermal Titration Calorimetry Investigation Resolves Conditions for Ligand Exchange and Phase Transformation in $CsPbBr_3$ Nanocrystals

Sakiru L. Abiodun, Megan Y. Gee, and Andrew B. Greytak*

Cite This: *J. Phys. Chem. C* 2021, 125, 17897−17905

Read Online

ACCESS | Metrics & More | Article Recommendations | Supporting Information

ABSTRACT: Inorganic halide perovskite nanocrystals (NCs), such as $CsPbBr_3$ quantum dots, have emerged as an intriguing alternative to traditional semiconductors in optoelectronic devices, but their rational development is hindered by limited stability, including reactions that lead to other solid phases at ambient conditions. Dimethyldidodecyl ammonium bromide (DDAB) is one of the most widely studied ligands in efforts to stabilize $CsPbBr_3$ NCs through surface modification. While some researchers have reported improved quantum yield, optoelectronic performance, and stability through such ligand exchange, others have reported it to cause a phase transformation to poorly fluorescent two-dimensional (2D) $CsPb_2Br_5$ nanoplatelets. Here, we investigated the thermodynamics of this ligand-mediated phase transformation of $CsPbBr_3$ NCs using absorption spectroscopy and matched NMR and isothermal titration calorimetry measurements. We were able to resolve two different processes that occur upon the introduction of DDAB. Ligand exchange, displacing native oleate and oleylammonium ligands, proceeds readily at low DDAB concentrations with an exchange equilibrium constant of ~10^2 and is endothermic with $\Delta H°$ ~30 kJ mol^{-1}. Larger equivalencies bring about a second process that is exothermic and corresponds to a displacement of $PbBr_x$ complexes from NC surfaces; these complexes ultimately lead to the formation of the 2D phase. Resolving these processes through a direct thermal measurement helps to reconcile contradictory conclusions in prior studies of surface passivation with quaternary ammonium bromides. In addition to revealing conditions that lead to instability of $CsPbBr_3$ NCs, the present findings could also guide the intentional formation of 2D $CsPb_2Br_5$ and 2D/3D $CsPbBr_3/CsPb_2Br_5$ composite structures of interest for selected applications.

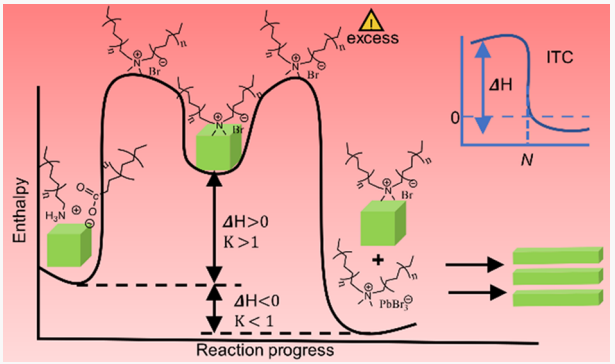

INTRODUCTION

Inorganic halide perovskite (IHP) nanocrystals (e.g., $CsPbX_3$: X = Br, Cl, I) have been the center of much attention in recent years due to their ease of preparation, high molar extinction coefficient, easily adjustable band gap energy via composition and size, narrow emission widths and excellent charge-transfer performance.[1−4] These unique properties make them an excellent choice in various optoelectronic devices such as sensors, solar cells, LEDs, lasers, photodetectors, field-effect transistors (FETs), and X-ray scintillators. However, progress in the incorporation of IHP nanocrystals (NCs) toward these applications is limited by difficulties with stability. Efforts to improve stability have focused on surface chemistry, for example, replacing the native ligand coating through ligand exchange reactions.[5] However, this approach has encountered challenges. For example, the introduction of amines and quaternary ammonium halides to replace native oleylammonium ligands has been shown to induce structural transformation of $CsPbX_3$ NCs[6−9] including the formation of other cesium-lead bromide phases, such as Cs_4PbBr_6 and $CsPb_2Br_5$. While undesirable if the goal is perovskite quantum dots, these phases have also gained considerable attention in their own right.[10−16] While the preparation of $CsPbBr_3$ NCs typically involves a direct synthesis, the other phases such as Cs_4PbBr_6 and $CsPb_2Br_5$ are often prepared through a chemical transformation of presynthesized $CsPbBr_3$ NCs. The ability to move among these phases under mild conditions is intriguing, and there has been much effort to understand these processes.[17−19] However, to date not enough is known about the mechanisms of these transformations. While some researchers have reported the transformation of $CsPbBr_3$ to $CsPb_2Br_5$ through water treatment,[19,20] or bromide precursor ($CsBr$ or $PbBr_2$) treatment,[21] others have reported a ligand-

Received: January 7, 2021
Revised: July 22, 2021
Published: August 9, 2021

mediated transformation.[6,7,22] Also, the presence of 2D $CsPb_2Br_5$ in $CsPbBr_3$ has been reported to enhance its ($CsPbBr_3$) stability against moisture by adopting a core−shell structure, especially for improved solar cell efficiency[23,24] via decreased trap density, which in turn causes improvement in carrier lifetime.[25] Moreover, $CsPbBr_3/CsPb_2Br_5$ composites have been reported in photodetector[26,27] and cell bio-imaging applications.[28] It is therefore important to investigate the chemistry of these transformations in more detail. The properties of alternative Cs−Pb−Br phases have generated some conflicting reports. While some have described $CsPb_2Br_5$ nanoplatelets with strong green emission,[12,29] others report $CsPb_2Br_5$ as having an indirect band gap of about 3.35 eV[30] with no visible PL.[19,30,31] In a recent article, Dahl et al. elucidated a weakly reversible phase diagram for Cs−Pb−Br nanomaterials including $CsPb_2Br_5$, $PbBr_2$ nanocrystals, and molecular lead halide species.[32] Therein, they showed that $CsPb_2Br_5$ possesses an absorption peak around 320 nm with an onset starting around 350 nm.

Among ligand exchange treatments, quaternary ammonium bromides have been found to be effective in passivating the surface of $CsPbBr_3$ NCs, but with some contradictory reports in literature. For example, didodecyldimethylammonium bromide (DDAB) has emerged as one of the most widely studied compounds employed to attempt to stabilize IHP nanocrystals through surface ligand exchange.[33−38] The quaternary ammonium ion is immune to loss of its charge through deprotonation, and yet the methyl-substituted headgroup is able to fit within the Cs vacancy site at the $CsPbBr_3$ NC surface.[33] While some researchers have reported the ligand to cause an improvement in stability and quantum yield,[33,34] others have reported it to cause a phase transformation from 3D $CsPbBr_3$ structure to 2D-layered $CsPb_2Br_5$ in the form of nanoplatelets (NPLs).[7] We have recently demonstrated that gel permeation chromatography (GPC) can be used to purify $CsPbBr_3$ NCs with native oleate/oleylammonium surface termination as well as the same NCs following ligand exchange with DDAB, with DDAB leading to improved QY and stability.[38] Therefore, identifying the reactions that take place upon DDAB treatment and the thermodynamics of each step is a promising avenue to a better understanding of the NC surface and reliable approaches to stable products. Previous efforts to obtain ligand binding and exchange thermodynamics have included variable-temperature NMR measurements,[5,39] and a study by Quarta et al. in which abatement of light scattering (due to improved dispersion) is used as a proxy for ligand binding to compare the binding of organic amines and ammonium salts with varying basicity, chain length, and steric hinderance to $CsPbBr_3$ NCs.[8] The same study reported improved dispersion with DDAB exposure at low concentration, crossing over to loss of band-edge absorbance at higher equivalency, but detailed measurements of DDAB exchange remain elusive.

Isothermal titration calorimetry (ITC) has been extensively used to study the thermodynamics of binding in proteins[40−44] and recently to study the surface chemistry of NCs by our group and others.[45−50] ITC has proved to be particularly valuable as a complementary technique to spectroscopic methods of analysis such as NMR, FTIR, and optical spectroscopies. ITC is feasible at lower concentrations than NMR and does not necessarily require a resolvable spectroscopic handle. Also, since ITC directly measures enthalpy changes, in some cases, the difference in enthalpy can be used to resolve different processes that occur when a ligand is introduced.[40,46] However, the power of ITC to measure reaction enthalpies is greatly strengthened when it can be combined with NMR or other spectroscopies to confirm the nature and extent of reaction over the course of the titration. Elimelech et al. used complimentary ITC and NMR analysis to study ligand exchange reactions of oleate-capped CdSe NCs to a variety of alkyl thiols.[47] Calvin et al. used similar techniques to investigate the thermodynamics of reaction of treatments of InP NCs with metal halide salts and phosphonic acids.[49,50]

Here, we studied the quantitative ligand exchange of oleate/oleylammonium-capped $CsPbBr_3$ NCs with DDAB and subsequent ligand-mediated transformations toward 2D $CsPb_2Br_5$ under excess DDAB conditions, using complementary techniques of absorption spectroscopy, solution NMR, and isothermal titration calorimetry (ITC). Our surface analysis has been able to resolve simultaneous equilibria for ligand exchange and surface etching that govern the progress of the reaction as DDAB is introduced to purified $CsPbBr_3$ NCs. In addition to this, we also found that the formation of 2D $CsPb_2Br_5$ nanoplatelets is accelerated by further increases in the concentration of DDAB beyond the necessary amount for effective passivation of the NC surface. Our approach in what follows was to successively introduce aliquots of a DDAB stock solution to natively capped $CsPbBr_3$, formed from oleate/oleylamine stabilized precursors, in a toluene solution. The effect of this treatment was examined by parallel NMR and ITC experiments.

METHODS

Materials. All chemicals were used as received unless otherwise stated. Ethanol (200 proof) was purchased from Decon Laboratories; toluene (99.9%) was purchased from Fisher Scientific. Bio-Beads S-X1 GPC medium was obtained from Bio-Rad Laboratories. Toluene-d_8 (99.5%) was purchased from Cambridge Isotope Laboratories. 1-Octadecene (ODE, 90%) and oleylamine (OAm, 80−90%) were purchased from Acros Organics. Oleic acid (OA, 99%), $PbBr_2$, and Cs_2CO_3 were obtained from Alfa Aesar. DDAB was purchased from BTC chemicals.

Cesium Oleate (CsOA) Synthesis. Typically, 0.2040 g of Cs_2CO_3, 0.777 g of OA, and 5.85 g of ODE were loaded into a 25 mL three-round neck bottom flask and dried under vacuum at 120 °C for 1 h. The temperature was then raised to 150 °C under flowing N_2 until a clear solution of CsOA is obtained.

$CsPbBr_3$ NC Synthesis. NCs were synthesized as described previously.[38] Briefly, 144 mg of $PbBr_2$, 1 mL of OA, 1 mL of OAm, and 7.5 mL of ODE were loaded onto a 25 mL three-neck round bottom flask, then dried for 1 h under vacuum. The Schlenk line was switched to N_2 and temperature was raised to 190 °C. One milliliter of presynthesized CsOA (at 150 °C) was then rapidly injected and the flask immediately cooled under an ice bath. The crude synthesized mixture was then centrifuged at 10 000 rpm for 5 min, and the supernatant discarded. The precipitate is redispersed in 3 mL of toluene and recentrifuged at 10 000 rpm for 10 min. The NC solution in toluene was then carefully pipetted into a clean vial and stored until needed.

Ion Metathesis Preparation of PF_6^- Salts. DDAB or tetraoctylammonium bromide (TOAB) is first dissolved in toluene followed by the addition of a slight excess of potassium hexafluorophosphate (KPF_6) and thoroughly mixed for 30 min, leading to precipitation of KBr. The mixture is then

https://doi.org/10.1021/acs.jpcc.1c00144
J. Phys. Chem. C 2021, 125, 17897−17905

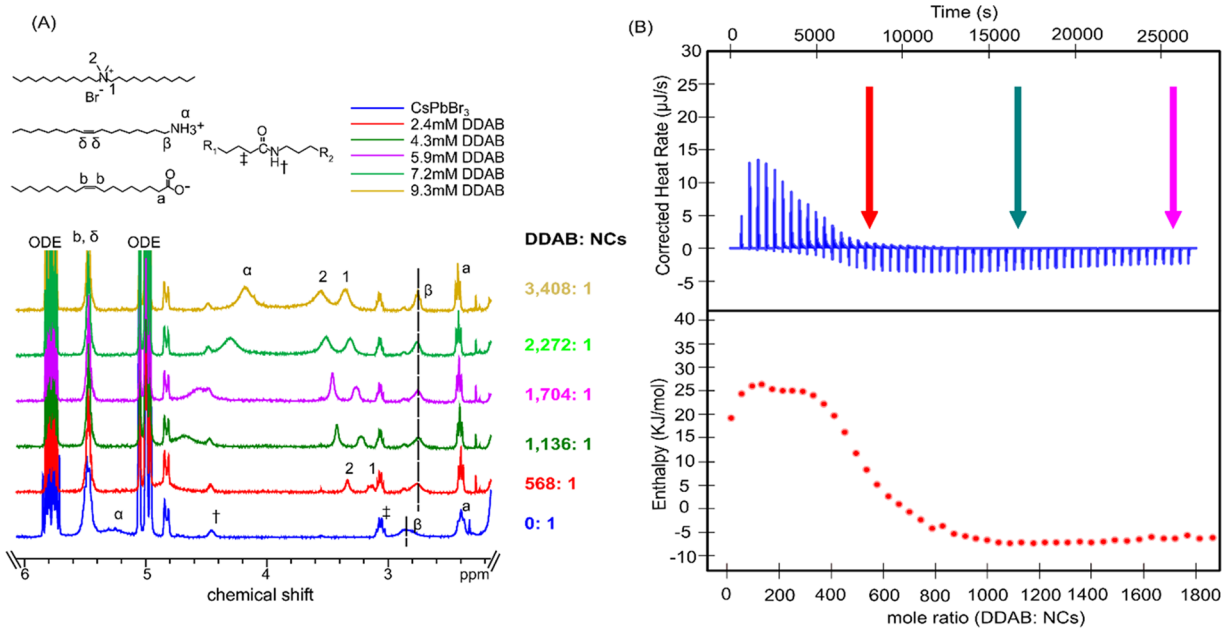

Figure 1. (A) ^{1}H NMR spectra showing displacement of oleic acid and oleylamine from the surface of $CsPbBr_3$ NCs in the presence of increasing DDAB concentration. (B) Baseline-corrected ITC thermogram (top) and corresponding integrated enthalpy change per mole of reactant (bottom) for titration of DDAB into $CsPbBr_3$. Mole ratios corresponding to the first three NMR titration points are indicated by the arrows.

filtered to remove KBr and undissolved KPF_6, while organic hexafluorophosphate compounds ($DDA^+PF_6^-$ or $TOA^+PF_6^-$) remain in the solution.

GPC Purification. A GPC column was prepared and equilibrated with toluene as described previously.[38,51] A column height of approximately 30 cm was employed. For purification, typically, 1 mL of NCs was centrifuged at 10 000 rpm and then carefully loaded unto the GPC column, followed by elution by addition of clean toluene mobile phase.

^{1}H NMR Analysis of NCs. All NMR spectra were recorded on a Bruker Avance III-HD 400 MHz spectrometer. NMR spectra of $CsPbBr_3$ NCs were taken in deuterated toluene-d_8.

NMR Titration. For NMR titration, 0.4 mL of 4.76 μM solution of $CsPbBr_3$ NCs was pumped dry under vacuum, redispersed in deuterated toluene-d_8, and pipetted into an NMR tube. For the first−fourth titration, 50 μL of 0.0216 M DDAB solution (in toluene) is added to the NMR tube, which was then shaken to promote mixing. For the last titration, 100 μL 0.0216 M DDAB was added.

Isothermal Titration Calorimetry. ITC titrations were performed on a TA-instrument Nano-ITC Standard Volume calorimeter. Ligand solutions were titrated from a 250 μL syringe into the sample cell, which was overfilled to its capacity of about 1.2 mL (active volume 950 μL). The initial NC concentration was 0.5 μM. The reference cell was filled with pure toluene. For each experiment, auto-equilibration was followed by an additional 600 s delay. To allow for equilibration between each injection, a 480 s time interval was set between each injection for a total of 55 injections at 4.57 μL injection volume (calibrated: 4.5 μL nominal). The first injection was set to 2.0 μL and the first two points were excluded from the thermodynamic fit to account for possible premixing of the syringe solutions during the equilibration time. Reference titrations of the ligand solution were titrated into a clean toluene solvent, performed to detect any significant heat of dilution. Although the reference signal was small, it was subtracted from actual NC titration isotherms before analysis. All heat signals obtained were fitted using identical independent sites (Langmuir) using NanoAnalyze or using the two-site exchange model implemented in custom MATLAB code.

Transition Electron Microscopy. TEM images were recorded with a Hitachi H-8000 microscope for all samples. Diluted NC solutions in toluene were drop casted onto 400 mesh Cu grids with an ultrathin carbon support film (Type-9A, Ted Pella, Inc.) and pumped dry under vacuum for 30 min prior to imaging.

RESULTS AND DISCUSSION

For the present study, cuboidal $CsPbBr_3$ NCs with edge length ~6.7 nm were synthesized using a modified hot injection method similar to previous reports.[52,53] Following synthesis, the QDs flocculate spontaneously from the ODE solvent and could be recovered by centrifugation; they were then brought into solution in toluene for storage and further investigation. We have recently demonstrated that such NCs possess a native oleate/oleylammonium ligand coating, and that their QY and stability can be improved through the introduction of DDAB in toluene solvent.[38]

^{1}H NMR Results. Figure 1A illustrates a ^{1}H NMR titration conducted to investigate the effect of DDAB addition to the NCs in toluene. For this experiment, a portion of the QD sample was taken to vacuum and brought into toluene-d_8. The NC concentration was determined from the molar extinction coefficient as described by de Roo et al.[54] Starting with 0.4 mL of a ~4.76 μM $CsPbBr_3$ NC sample, aliquots of a DDAB stock solution were sequentially added leading to the total concentrations indicated. The corresponding mole ratio of total DDAB/NC added is also indicated alongside each spectrum. Each titration was also followed by UV−vis absorption spectroscopy (Figure S1). The assignment of the NMR features is summarized in Figure 1A. Spectra for free ligands in toluene-d_8 are provided in Supporting Information Figures S3 and S4 for comparison. The peaks labeled † and ‡

https://doi.org/10.1021/acs.jpcc.1c00144
J. Phys. Chem. C 2021, 125, 17897−17905

Scheme 1. Reaction of DDAB with $CsPbBr_3$ Nanocrystals

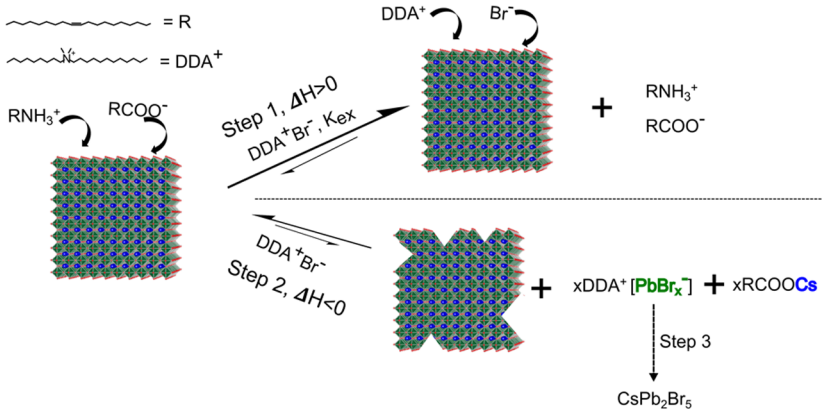

correspond to an amide condensed from OA and OAm; they do not change significantly during the NMR titration, which indicates that they are not interacting with the surface of NCs. Similar results have been observed in literature.[55]

To monitor displacement of native ligands from the surface of the NC, we focused on peaks labeled "a" and "β" of the oleic acid and oleylamine, respectively. The oleic acid "a" peak collapses from being a broad peak to a sharp triplet while the peak labeled "β" also migrated upfield (from 2.86 to 2.74 ppm, matching the free ligand) and became sharper after the first DDAB titration. Typically, bound ligand NMR resonances are broadened and show downfield migration of peaks compared to those of free ligands in solution.[55] Consequently, the changes in *a* and *b* are characteristics of the ligands dissociated from the NC surface,[55] indicating that oleate and oleylammonium ion ligands are being substantially displaced from the surface upon the first injection of DDAB. There are no significant changes in the line shape and position of the peak labeled "a" and "β" for subsequent DDAB addition after the first titration. This suggests that the ligand exchange has already approached completion after the first titration.

Peaks labeled 1 and 2 are associated with methyl and methylene protons nearest the nitrogen in the DDA^+ cation. We note that these peak positions have been shown to be concentration dependent in the absence of NCs: Imran et al.[33] observed continuous downfield migration and broadening of these peaks as the concentration of DDAB is increased in toluene solution, similar to our observation in Figure 1A. Therefore, the position and shape of the peaks (2 and 1) are unreliable indicators of the progress of ligand exchange as they depend on the final concentration in solution.[33] Nevertheless, we and others have noted retention of these DDAB resonances in NMR of purified NCs following exchange of native ligands with DDAB at comparable concentrations, indicating significant binding to the NC surface.[33,38] In a similar vein, the peak labeled α is an acidic proton that could also undergo a fast proton exchange in solution during each addition of DDAB (e.g., $RNH_3^+ + Br^- \leftrightarrow RNH_2 + HBr$), thus explaining its continuous migration during each DDAB addition.

Observation of the UV−vis absorption spectrum during the NMR titration (as shown in the Supporting Information, Figure S1) reveals a change in the absorption profile around 310 nm that is evident even after the first DDAB addition (50 μL added, equivalent to 568 DDAB/NC), and an additional, broader absorption with an onset around 355 nm that appears after the last addition. We ascribe these absorption peaks to the formation of $DDA^+[PbBr_3^-]$ complexes and $CsPb_2Br_5$ NPLs, respectively, based on past literature reports.[7,32,56] In particular, similar absorption profiles have been reported with these assignments by Balakrishnan et al.[7] and by Dahl et al.[32] Notably, the bright visible green photoluminescence (PL) of the initial $CsPbBr_3$ NC sample became quenched after the last titration.

Analysis of $CsPbBr_3$ NCs exposed to a similar excess of DDAB with transmission electron microscopy (TEM, Figure S2) revealed platelets that were absent from the NC samples prior to DDAB exposure. To further clarify the ligand exchange process as observed by NMR, we repeated the DDAB NMR titration using a GPC-purified NC sample (see Figure S5 for details), which revealed a similar trend indicative of ligand exchange of native oleate and oleylammonium, followed by continued shifts in DDAB peak positions at higher equivalencies. The similar ligand exchange behavior before and after GPC purification supports coordination of the NC surface by oleate and oleylammonium ligands in the initial sample and further indicates that the GPC-purified sample can be an appropriate starting point for thermodynamic investigation of ligand exchange with a minimum of solution-phase impurities.

Based on the observation from our NMR result and past reports,[7,34] we proposed a reaction scheme (Scheme 1) occurring on the surface of the NC. There are three steps: step 1 involves ligand exchange of native ligands to $DDA^+ Br^-$, step 2 involves the etching of the NC to form a $DDA^+[PbBr_3^-]$ complex, while step 3 corresponds to the formation of NPLs from the corresponding products formed from step 2.

ITC Results. Having identified these two regimes via the ^1H NMR spectra, we sought to understand in more detail the thermodynamics of the ligand exchange, as well as the subsequent process ultimately leading to phase transformation of $CsPbBr_3$ to Cs_2PbBr_5, via ITC. To minimize the possible interference of impurities on the calorimetry results, natively capped $CsPbBr_3$ NCs were purified using gel permeation chromatography (GPC).

The GPC-purified sample is then loaded onto the sample cell of the ITC, with the reference cell being filled with pure toluene. A known concentration of DDAB (3.0 mM in toluene) was prepared in a glove box and loaded onto the titrant syringe (see the Methods section for details). Figure 1B shows the raw heat signal (thermogram) and the corresponding integrated heat (isotherm) generated from a representative ITC titration with DDAB at 3.0 mM. Titrations were done in

https://doi.org/10.1021/acs.jpcc.1c00144
J. Phys. Chem. C 2021, 125, 17897−17905

triplicate. First, two titrations were done under identical conditions (using 3.0 mM DDAB) to check the reproducibility of the result, while the third titration was done using a higher titrant concentration of 6.0 mM to confirm appropriate scaling of the result with titrant concentration and extend to higher ultimate DDAB equivalency.

The ITC signal in Figure 1B clearly indicates contributions from at least two distinct processes: one endothermic and the other exothermic. This is evidenced in the change of the integrated heat signal from positive (endothermic) to negative and in the appearance of different waveform shapes in the raw heat thermogram between the beginning and end of the experiment. The endothermic process concludes relatively abruptly, which is characteristic of saturation of strongly binding sites, while the exothermic signal diminishes only slowly with successive titration points as might be expected for a weaker interaction. Isotherms generated from additional replicate titrations are presented in the Supporting Information (Figure S7). The results are highly consistent and yield similar thermodynamic model parameters on analysis, as discussed below.

Under favorable conditions, ITC can distinguish and resolve different types of binding sites in biological systems and also for NCs.[46,47,57] Based on supporting evidence from the NMR titration (indicating substantially complete ligand exchange by ~568 mole ratio, Figure 1A,B), we attribute the endothermic contribution to the isotherm to ligand exchange at the NC surface with DDA^+/Br^- displacing oleate and oleylammonium native ligands (step 1 as illustrated in Scheme 1). The exothermic contribution that commences as the first process is reaching completion we attribute to the displacement of Pb-containing complexes from the surface (represented as $DDA^+PbBr_x^-$ in step 2 of Scheme 1). Our reaction scheme is in agreement with past reports that consider the NC as being composed of $[CsPbBr_3](PbBr_2)\{AX'\}$, where $[CsPbBr_3]$ represents a stoichiometric inner core, surrounded by a $PbBr_2$ monolayer and a mixed anion/cation coordination layer occupying Cs and Br sites.[58,59]

Figure 2 shows representative absorption spectra and TEM images of the sample before and after ITC. The sample recovered from ITC (approximately 12 h after the start of the reaction; ultimate total [DDAB] ≈ 450 μM) shows elevated

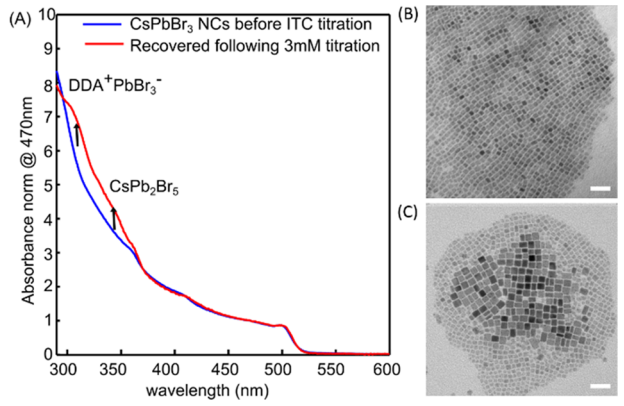

Figure 2. (A) Normalized UV−vis spectra before and after ITC titration showing the formation of new absorption features with time. (B) TEM image before ITC titration showing cuboid NCs. (C) TEM image after ITC showing the prevalence of larger and more irregularly shaped NCs due to ripening. Scale bars, 40 nm.

absorption bands in the UV associated with $PbBr_3^-$ and $Pb_2Br_5^-$ complexes and/or $CsPb_2Br_5$,[7,32] along with a small red shift in the band-edge absorption peak of $CsPbBr_3$. Representative TEM micrographs (Figure 2B,C) indicate a larger and broader size distribution of cuboid shapes, suggesting that solubilization of $PbBr_x^-$ has promoted Ostwald ripening. Our observation from the absorption spectra of the solution of NCs recovered after ITC over time shows that nanoplatelets are formed over a period of time rather than instantaneously upon injection of DDAB. This has also been observed by other groups.[7,34] Therefore, the exothermic signal observed in the ITC, which reaches equilibrium rapidly as seen in the thermogram traces, must be from the formation of an intermediate (step 2 of Scheme 1). Step 3 of the reaction scheme (in which ripening and NPL formation occur via PbBrx complexes displaced in step 2) proceeds slowly, unobserved in the ITC trace, and could involve precipitation and/or formation of different side products. In fact, upon examining the samples recovered from ITC titration using 3 mM DDAB after a much longer time period (up to 6 months), we found 340 nm absorbance signal continued to increase over time, with a corresponding decrease in the absorption edge of $CsPbBr_3$ NCs (Figure S6), indicating continued etching of nanocrystals and corresponding transformation into $Pb_2Br_5^-$ and/or $CsPb_2Br_5$ NPLs. The partial overlap of steps 1 and 2 (Figure 1B) appears to show that these two processes occur in a thermodynamically simultaneous manner, rather than in a sequential (conditional) one, but the first process takes place more significantly at the beginning of the titration indicative of a larger effective association equilibrium constant.

When we repeated the ITC titration with higher DDAB concentration (6 mM instead of 3 mM titrant: ultimate total [DDAB] ≈ 900 μM), the endothermic signal (step 1) completes at the same mole ratio of DDAB added per NC, while the exothermic signals (etching of the NC: step 2) continue over the entire titration (Figure S7). As shown in Figure 3, an inspection of the recovered sample after ~12 h

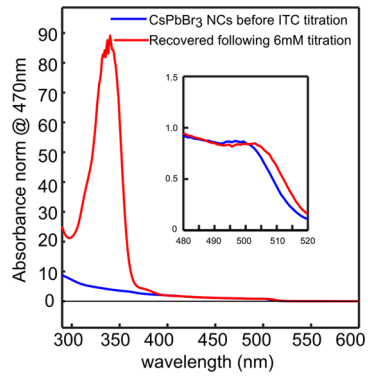

Figure 3. Normalized UV−vis spectra before and after ITC using a higher concentration of DDAB (6 mM titrant, final conc. ≈900 μM), indicating accelerated morphological changes at high equivalency.

showed that the transformation from $CsPbBr_3$ to $CsPb_2Br_5$ (step 3) occurred far more rapidly and extensively under the conditions found at the conclusion of this titration, similarly to what was observed at high [DDAB] in the NMR titration samples.

Thermodynamic Analysis. To obtain parameters for the ligand exchange reaction in step 1 from the ITC data, the simplest approach is to model it as competitive binding at a

https://doi.org/10.1021/acs.jpcc.1c00144
J. Phys. Chem. C 2021, 125, 17897−17905

single set of identical independent sites initially occupied by native ligands (site 1). The chemical equation for this step and the corresponding equilibrium constant K_{ex} are represented in eqs 1 and 2 below, where θ_1 is the fractional occupancy of site 1 by the new ligand:

$$\mathrm{NC(RNH_3^+ - RCO_2^-)} + \mathrm{DDA^+ - Br^-} \leftrightarrow$$
$$\mathrm{NC(DDA^+ - Br^-)} + \mathrm{RNH_3^+ - RCO_2^-} \quad (1)$$

$$K_{ex} = \frac{[\mathrm{NC(DDA^+ - Br^-)}][\mathrm{RNH_3^+ - RCO_2^-}]}{[\mathrm{NC(RNH_3^+ - RCOO^-)}][\mathrm{DDAB}]} = \frac{\theta_1}{(1-\theta_1)}\frac{[\mathrm{L_1}]}{[\mathrm{DDAB}]} \quad (2)$$

We have shown previously that the competitive binding isotherm for a 1:1 ligand exchange, in the limit of a large exchange equilibrium constant K_{ex} with negligible free ligand or vacant sites to start with, can be approximated in terms of a Langmuir isotherm with effective association constant K_{eff}. A Langmuir-model fit of the data can provide K_{eff}, N, and ΔH from which K_{ex} can be obtained.

The presence of the second exothermic process complicates the application of this approach in the present case, as the equilibrium for each process must be satisfied simultaneously and titration points near the transition between them will contain heat contributions from each. Nevertheless, the step with the largest equilibrium constant will predominate at low equivalency. Inspection of the ITC isotherm (Figure 4) shows

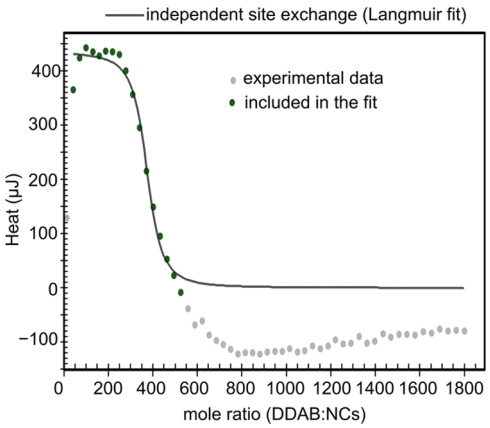

Figure 4. Fit of endothermic region of data in Figure 1B as ligand exchange at identical, independent sites.

that the exothermic signal seen at high equivalencies is due to a sharp exothermic wave that is largely absent from the signal at the beginning of the titration. Consequently, approximate values for the reaction parameters for site 1 (step 1), describing DDAB ligand exchange, can be obtained by selectively fitting the endothermic portion of the ITC isotherm using the Langmuir-model approximation. Figure 4 shows this fit for the titration shown in Figure 1B, and the site parameters obtained from the three replicates are summarized in Table 1.

As discussed above, the second step appears to entail displacement of $PbBr_x$ complexes from the NC surface. To resolve the contributions from step 1 and step 2 more precisely, we considered a model that explicitly describes the competitive binding of the same DDAB ligand component at two sets of thermodynamically distinct "sites" with site 1 representing oleate/oleylamine exchange and site 2 accounting for the displacement of PbBrx from the NC surface in step 2. As discussed in the Supporting Information, for values of $K_{ex} \ll 1$, ITC isotherms for competitive ligand exchange are parameterized by a single value: the product $\Delta H(NK_{ex})^{1/2}$, and as such, unique values for ΔH_2, N_2, and K_{ex2} are not easily obtained from the data alone. Based on the scaling of the incremental heat with injection number (or mole ration of DDAB/NCs), step 2 appears to fall in this regime. Given this limitation and the complexity of the reaction, we are hesitant to draw conclusions about the equivalency or reaction parameters for the second step, but we have clearly shown that it proceeds with a much smaller equilibrium constant than step 1 (ligand exchange).

Closer inspection of the first few titration points in Figure 1B and each of the replicates in the Supporting Information (Figure S7) shows that the integrated heat signal is initially diminished and grows larger (more endothermic) before eventually falling as step 1 saturates. This behavior can be a signature of competitive binding reactions that start with a few vacant sites due to low equivalency of the initial ligand, but could also arise from ligand interactions.

To investigate this region in more detail, and also to separate the influence of cationic (DDA^+ for oleylammonium) and anionic (Br^- for oleate) ligand exchange on the overall result when DDAB is introduced, we repeated ITC titrations at lower equivalency (DDAB:NC between 1 and 650) focusing on the ligand exchange region. This allowed us to compare ITC titration results for DDAB and analogous salts in which weakly interacting counterions are substituted: tetraoctylammonium bromide (TOAB), didodecyldimethylammonium hexafluorophosphate ($DDA^+PF_6^-$), and $TOA^+PF_6^-$ (Figures S9 and S10). As shown in the Supporting Information (Figure S11), the rising and falling endothermic signal is seen when DDAB and $DDA^+PF_6^-$ are introduced. In contrast, TOAB generated a classically sigmoidal endothermic isotherm, saturating at similar total equivalency. $TOA^+PF_6^-$ showed a smaller endothermic signal indicative of weak interactions. The conclusion is that both anionic and cationic exchanges are endothermic in this reaction. Also, the initial rise in the isotherms for the DDA^+ titration indicates the occupation of initially vacant sites. Following GPC purification, it is likely that NCs have some Cs/Br vacancies that are not occupied by the native organic ligands due to the removal of excess ligands during GPC purification. The initially diminished endothermic response when DDA^+ is introduced could indicate that DDA^+/Br^- and DDA^+/PF_6^- are able to occupy these sites initially without displacing the native ligands in which the DDA^+ occupy the Cs vacancy. In contrast, TOA^+ being a very bulky ligand is unable to occupy these Cs vacancies. As a result, Br^- does not bind to vacant sites when accompanied by the bulkier TOA^+ and can only bind by displacing OA^-. Adding together control titrations gives an isotherm that approximates, but overestimates, the DDAB isotherm: the difference could indicate more favorable interligand interactions in the DDA^+/Br^- coating than are achieved when only one is exchanged, which is plausible given the steric bulk of both oleate and oleylammonium. The presence of significant interligand interactions, which is not unexpected for NC surfaces, indicates that the parameters resulting from the Langmuir fit must be considered as effective values that implicitly incorporate such interactions, given the crudeness of the Langmuir-model approximation in the present case, but they

https://doi.org/10.1021/acs.jpcc.1c00144
J. Phys. Chem. C 2021, 125, 17897−17905

Table 1. Thermodynamic Parameters for Ligand Exchange of 6.7 nm OA/OAm-Capped $CsPbBr_3$ NCs with DDAB

	K_{ex}	N (per NC)	ΔH (kJ mol^{-1})	ΔS (J mol^{-1} K^{-1})	ΔG (kJ mol^{-1})
site 1	130 ± 55[a]	343 ± 13[a]	32.7 ± 4.0[a]	150 ± 13[b]	−12.1 ± 1.0[b]

[a]Uncertainty represents the standard deviation for ITC fit parameters on three replicate titrations. [b]Uncertainty represents propagated error.

can be a starting point for comparison with theoretical analysis and subsequent studies.

The K_{ex} of the ligand exchange (step 1) indicates that the binding of DDAB to the surface is favorable compared to the oleate/oleylammonium native ligand set. Using the equations $\Delta G^\circ = -RT \ln K$ and $\Delta G^\circ = \Delta H^\circ - T\Delta S^\circ$, the standard free energy change was estimated to be around −12.1 ± 1.0 kJ mol^{-1}. The endothermic initial ligand exchange is found to be driven by a large and positive entropy change, presumably driven by the release of oleylamine and oleic acid ligands into the toluene solution phase. Indeed, Imran et al.,[33] through their theoretical calculations, predicted that the difference in enthalpy is not the driving force for the greater stability of DDAB-capped surfaces, and our experimental evidence corroborates this result.

To compare the results from the NMR and ITC titrations, we revisited our NMR results using our thermodynamic model for the two-site exchange. Using the thermodynamic parameters from the ITC experiments, but substituting NC and ligand concentrations for the first NMR titration point (4.76 μM NC and 2.4 mM DDAB), we predict θ_1 = 97.6% occupation of site 1 with DDAB. Inspection of the NMR spectra of the first DDAB titration showed that indeed the upfield migration of the peak labeled β (for OAm^+) and the sharpening of the oleate "a" peak, characteristics of ligands displaced from the surface of NCs, is essentially complete at this point. As discussed previously, after the first titration, these two peaks show no significant change. At this same titration point, step 2, corresponding to the $DDA^+PbBr_3^-$ complex formation, has proceeded to only a small extent ($\theta_2 \approx 7\%$ in the two-site model).

We note that the Infante group, in a computational study, predicted that stripping the outer core ($PbBr_2$) of the NC (corresponding to etching of the NC: step 2 of Scheme 1) could lead to considerable reorganization of the NC.[59] This shows that performing a ligand exchange with a relatively larger amount of DDAB (more than necessary for the passivation of the surface of the nanocrystals, 1.3 ligands/nm^2 based on measured N for site 1) will accelerate the rate of transformation of nanocrystals. This result clearly shows that DDAB can serve as a ligand for effective passivation[33,60] and yet also be a driver for phase transformation, corroborating the earlier reports that excess DDAB is detrimental to the surface of $CsPbBr_3$ NCs.[8] The sensitivity of the phase transformation rate to the excess DDAB concentration, which bears a resemblance to that noted by the Kamat group for exposure of $CsPbBr_3$ NCs to dodecyldimethylamine,[7] could indicate the presence of a nucleation threshold for the concentration of the soluble complex that is formed by the exothermic process in the ITC results, above which precipitation of CsBr and/or $CsPb_2Br_5$ is accelerated.

CONCLUSIONS

We have successfully separated and quantified the thermodynamics of two different processes that occur during DDAB treatment of initially oleate/oleylammonium-capped $CsPbBr_3$ NCs: namely, ligand exchange that proceeds readily with a large equilibrium constant, followed by a ligand-mediated displacement reaction that ultimately leads to phase transformation of $CsPbBr_3$ NCs to 2D $CsPb_2Br_5$. In light of these conclusions, an effective strategy for using quaternary ammonium halide treatment to produce highly stable and fluorescent $CsPbBr_3$ NCs is to conduct ligand exchange with only a modest excess to drive the first step, followed by removal of excess DDAB and displaced oleic acid/oleylamine native ligands, so that steps 2 and 3 cannot advance significantly at equilibrium. We have recently implemented a variant of this approach using GPC purification following DDAB exchange to isolate stabilized NCs.[38] Understanding the thermodynamics of the phase transformation pathway should also help provide better-targeted approaches for intentional formation of $CsPb_2Br_5$ nanomaterials including epitaxial core−shell structures. Also, ITC has proven to be a highly effective complementary technique for understanding surface reactions in NCs and has been used to probe the surface chemistry of chalcogenide NCs,[46−48] but until now had not yet been applied to the surface reactions of perovskite NCs. We anticipate that the versatility of this technique in understanding surface reactions in NCs could be useful in studying other surface and bulk reactions in IHP NCs in the near future, with prospects for improving their stability and optoelectronic performance.

ASSOCIATED CONTENT

Supporting Information

The Supporting Information is available free of charge at https://pubs.acs.org/doi/10.1021/acs.jpcc.1c00144.

Details of the thermodynamic model for ligand exchange at one and at two simultaneous sets of sites; additional TEM images, UV−vis and NMR spectra; Langmuir fit; replicate ITC titrations; ligand to solvent control titration; Table S1; and Figures S1−S11 (PDF)

AUTHOR INFORMATION

Corresponding Author

Andrew B. Greytak − *Chemistry and Biochemistry, University of South Carolina, Columbia, South Carolina 29208, United States;* orcid.org/0000-0001-8978-6457; Email: greytak@mailbox.sc.edu

Authors

Sakiru L. Abiodun − *Chemistry and Biochemistry, University of South Carolina, Columbia, South Carolina 29208, United States;* orcid.org/0000-0002-6016-1215

Megan Y. Gee − *Chemistry and Biochemistry, University of South Carolina, Columbia, South Carolina 29208, United States*

Complete contact information is available at: https://pubs.acs.org/10.1021/acs.jpcc.1c00144

Notes

The authors declare no competing financial interest.

■ ACKNOWLEDGMENTS

This project was supported by the US NSF under awards CHE-1613388 and CHE-2109064, with additional support to S.L.A. from the University of South Carolina Office of Research through the SPARC program. The authors thank Dr. Adam Roberge and Dr. Vitaly Rassolov for helpful discussions and advice.

■ ABBREVIATIONS

GPC, gel permeation chromatography; IHP, inorganic halide perovskite; NC, nanocrystal; ITC, isothermal titration calorimetry

■ REFERENCES

(1) Wheeler, L. M.; Sanehira, E. M.; Marshall, A. R.; Schulz, P.; Suri, M.; Anderson, N. C.; Christians, J. A.; Nordlund, D.; Sokaras, D.; Kroll, T.; et al. Targeted Ligand-Exchange Chemistry on Cesium Lead Halide Perovskite Quantum Dots for High-Efficiency Photovoltaics. *J. Am. Chem. Soc.* **2018**, *140*, 10504−10513.

(2) Tan, Y.; Zou, Y.; Wu, L.; Huang, Q.; Yang, D.; Chen, M.; Ban, M.; Wu, C.; Wu, T.; Bai, S.; et al. Highly Luminescent and Stable Perovskite Nanocrystals with Octylphosphonic Acid as a Ligand for Efficient Light-Emitting Diodes. *ACS Appl. Mater. Interfaces* **2018**, *10*, 3784−3792.

(3) Xu, Y.; Chen, Q.; Zhang, C.; Wang, R.; Wu, H.; Zhang, X.; Xing, G.; Yu, W. W.; Wang, X.; Zhang, Y.; et al. Two-Photon-Pumped Perovskite Semiconductor Nanocrystal Lasers. *J. Am. Chem. Soc.* **2016**, *138*, 3761−3768.

(4) Liu, X.; Kuang, W.; Ni, H.; Tao, Z.; Huang, Q.; Chen, J.; Liu, Q.; Chang, J.; Lei, W. A Highly Sensitive and Fast Graphene Nanoribbon/$CsPbBr_3$ Quantum Dot Phototransistor with Enhanced Vertical Metal Oxide Heterostructures. *Nanoscale* **2018**, *10*, 10182−10189.

(5) Smock, S. R.; Chen, Y.; Rossini, A. J.; Brutchey, R. L. The Surface Chemistry and Structure of Colloidal Lead Halide Perovskite Nanocrystals. *Acc. Chem. Res.* **2021**, *54*, 707−718.

(6) Palazon, F.; Almeida, G.; Akkerman, Q. A.; De Trizio, L.; Dang, Z.; Prato, M.; Manna, L. Changing the Dimensionality of Cesium Lead Bromide Nanocrystals by Reversible Postsynthesis Transformations with Amines. *Chem. Mater.* **2017**, *29*, 4167−4171.

(7) Balakrishnan, S. K.; Kamat, P. V. Ligand Assisted Transformation of Cubic $CsPbBr_3$ Nanocrystals into Two-Dimensional CsPb2Br5 Nanosheets. *Chem. Mater.* **2018**, *30*, 74−78.

(8) Quarta, D.; Imran, M.; Capodilupo, A.-L.; Petralanda, U.; van Beek, B.; De Angelis, F.; Manna, L.; Infante, I.; De Trizio, L.; Giansante, C. Stable Ligand Coordination at the Surface of Colloidal $CsPbBr_3$ Nanocrystals. *J. Phys. Chem. Lett.* **2019**, *10*, 3715−3726.

(9) Toso, S.; Baranov, D.; Manna, L. Metamorphoses of Cesium Lead Halide Nanocrystals. *Acc. Chem. Res.* **2021**, *54*, 498−508.

(10) Akkerman, Q. A.; Park, S.; Radicchi, E.; Nunzi, F.; Mosconi, E.; De Angelis, F.; Brescia, R.; Rastogi, P.; Prato, M.; Manna, L. Nearly Monodisperse Insulator Cs4PbX6 (X = Cl, Br, I) Nanocrystals, Their Mixed Halide Compositions, and Their Transformation into $CsPbX_3$ Nanocrystals. *Nano Lett.* **2017**, *17*, 1924−1930.

(11) Liu, Z.; Bekenstein, Y.; Ye, X.; Nguyen, S. C.; Swabeck, J.; Zhang, D.; Lee, S.-T.; Yang, P.; Ma, W.; Alivisatos, A. P. Ligand Mediated Transformation of Cesium Lead Bromide Perovskite Nanocrystals to Lead Depleted Cs4PbBr6 Nanocrystals. *J. Am. Chem. Soc.* **2017**, *139*, 5309−5312.

(12) Wang, K.-H.; Wu, L.; Li, L.; Yao, H.-B.; Qian, H.-S.; Yu, S.-H. Large-Scale Synthesis of Highly Luminescent Perovskite-Related $CsPb_2Br_5$ Nanoplatelets and Their Fast Anion Exchange. *Angew. Chem., Int. Ed.* **2016**, *55*, 8328−8332.

(13) Yu, X.; Wu, L.; Hu, H.; Chen, M.; Tan, Y.; Yang, D.; Pan, Q.; Zhong, Q.; Supasai, T.; Zhang, Q. Cs_4PbX_6 (X = Cl, Br, I) Nanocrystals: Preparation, Water-Triggered Transformation Behavior, and Anti-Counterfeiting Application. *Langmuir* **2018**, *34*, 10363−10370.

(14) Acharyya, P.; Pal, P.; Samanta, P. K.; Sarkar, A.; Pati, S. K.; Biswas, K. Single Pot Synthesis of Indirect Band Gap 2D $CsPb_2Br_5$ Nanosheets from Direct Band Gap 3D $CsPbBr_3$ Nanocrystals and the Origin of Their Luminescence Properties. *Nanoscale* **2019**, *11*, 4001−4007.

(15) Liu, M.; Zhao, J.; Luo, Z.; Sun, Z.; Pan, N.; Ding, H.; Wang, X. Unveiling Solvent-Related Effect on Phase Transformations in CsBr−$PbBr_2$ System: Coordination and Ratio of Precursors. *Chem. Mater.* **2018**, *30*, 5846−5852.

(16) Li, J.; Zhang, H.; Wang, S.; Long, D.; Li, M.; Guo, Y.; Zhong, Z.; Wu, K.; Wang, D.; Zhang, T. Synthesis of All-Inorganic $CsPb_2Br_5$ Perovskite and Determination of Its Luminescence Mechanism. *RSC Adv.* **2017**, *7*, 54002−54007.

(17) Wu, L.; Hu, H.; Xu, Y.; Jiang, S.; Chen, M.; Zhong, Q.; Yang, D.; Liu, Q.; Zhao, Y.; Sun, B.; et al. Cs_4PbX_6 (X = Cl, Br, I) Nanocrystals to Highly Luminescent CsPbX3 Nanocrystals: Water-Triggered Transformation through a CsX-Stripping Mechanism. *Nano Lett.* **2017**, *17*, 5799−5804.

(18) Lou, S.; Zhou, Z.; Xuan, T.; Li, H.; Jiao, J.; Zhang, H.; Gautier, R.; Wang, J. Chemical Transformation of Lead Halide Perovskite into Insoluble, Less Cytotoxic, and Brightly Luminescent $CsPbBr_3$/$CsPb_2Br_5$ Composite Nanocrystals for Cell Imaging. *ACS Appl. Mater. Interfaces* **2019**, *11*, 24241−24246.

(19) Maity, G.; Pradhan, S. K. Composition Related Structural Transition between Mechanosynthesized $CsPbBr_3$ and $CsPb_2Br_5$ Perovskites and Their Optical Properties. *J. Alloys Compd.* **2020**, *816*, No. 152612.

(20) Turedi, B.; Lee, K. J.; Dursun, I.; Alamer, B.; Wu, Z.; Alarousu, E.; Mohammed, O. F.; Cho, N.; Bakr, O. M. Water-Induced Dimensionality Reduction in Metal-Halide Perovskites. *J. Phys. Chem. C* **2018**, *122*, 14128−14134.

(21) Pal, P.; Saha, S.; Banik, A.; Sarkar, A.; Biswas, K. All-Solid-State Mechanochemical Synthesis and Post-Synthetic Transformation of Inorganic Perovskite-Type Halides. *Chem. - Eur. J.* **2018**, *24*, 1811−1815.

(22) Shen, W.; Ruan, L.; Shen, Z.; Deng, Z. Reversible Light-Mediated Compositional and Structural Transitions between CsPbBr 3 and $CsPb_2Br_5$ Nanosheets. *Chem. Commun.* **2018**, *54*, 2804−2807.

(23) Song, P.; Qiao, B.; Song, D.; Liang, Z.; Gao, D.; Cao, J.; Shen, Z.; Xu, Z.; Zhao, S. Colour- and Structure-Stable CsPbBr3-$CsPb_2Br_5$ Compounded Quantum Dots with Tuneable Blue and Green Light Emission. *J. Alloys Compd.* **2018**, *767*, 98−105.

(24) Zhang, X.; Jin, Z.; Zhang, J.; Bai, D.; Bian, H.; Wang, K.; Sun, J.; Wang, Q.; Liu, S. F. All-Ambient Processed Binary $CsPbBr_3$−$CsPb_2Br_5$ Perovskites with Synergistic Enhancement for High-Efficiency Cs−Pb−Br-Based Solar Cells. *ACS Appl. Mater. Interfaces* **2018**, *10*, 7145−7154.

(25) Zhu, B.-S.; Li, H.-Z.; Ge, J.; Li, H.-D.; Yin, Y.-C.; Wang, K.-H.; Chen, C.; Yao, J.-S.; Zhang, Q.; Yao, H.-B. Room Temperature Precipitated Dual Phase CsPbBr3−CsPb2Br5 Nanocrystals for Stable Perovskite Light Emitting Diodes. *Nanoscale* **2018**, *10*, 19262−19271.

(26) Palazon, F.; Dogan, S.; Marras, S.; Locardi, F.; Nelli, I.; Rastogi, P.; Ferretti, M.; Prato, M.; Krahne, R.; Manna, L. From CsPbBr3 Nano-Inks to Sintered CsPbBr3−CsPb2Br5 Films via Thermal Annealing: Implications on Optoelectronic Properties. *J. Phys. Chem. C* **2017**, *121*, 11956−11961.

(27) Li, J.; Zhao, H.; Li, J.; Zheng, C.; Li, M.; Wang, S.; Ren, K.; Zhang, Y.; Yao, J. Photoresponse Properties and Energy Gap of CsPbBr3−CsPb2Br5 Compound Thin Film Prepared by One-Step Thermal Evaporation Method. *J. Mater. Sci.: Mater. Electron.* **2020**, *31*, 4956−4962.

(28) Lou, S.; Zhou, Z.; Xuan, T.; Li, H.; Jiao, J.; Zhang, H.; Gautier, R.; Wang, J. Chemical Transformation of Lead Halide Perovskite into Insoluble, Less Cytotoxic, and Brightly Luminescent $CsPbBr_3$/$CsPb_2Br_5$ Composite Nanocrystals for Cell Imaging. *ACS Appl. Mater. Interfaces* **2019**, *11*, 24241−24246.

https://doi.org/10.1021/acs.jpcc.1c00144
J. Phys. Chem. C 2021, 125, 17897−17905

(29) Tang, X.; Hu, Z.; Yuan, W.; Hu, W.; Shao, H.; Han, D.; Zheng, J.; Hao, J.; Zang, Z.; Du, J.; Leng, Y.; Fang, L.; Zhou, M. Perovskite $CsPb_2Br_5$ Microplate Laser with Enhanced Stability and Tunable Properties. *Adv. Opt. Mater.* **2017**, *5*, No. 1600788.
(30) Dursun, I.; Bastiani, De.; Turedi, M.; Alamer, B.; Shkurenko, B.; Yin, A.; El-Zohry, J.; Gereige, A. M.; AlSaggaf, I.; Mohammed, A.; Eddaoudi, O. F.; Bakr, M. $CsPb_2Br_5$ Single Crystals: Synthesis and Characterization. *ChemSusChem* **2017**, *10*, 3746−3749.
(31) Li, G.; Wang, H.; Zhu, Z.; Chang, Y.; Zhang, T.; Song, Z.; Jiang, Y. Shape and Phase Evolution from CsPbBr3 Perovskite Nanocubes to Tetragonal $CsPb_2Br_5$ Nanosheets with an Indirect Bandgap. *Chem. Commun.* **2016**, *52*, 11296−11299.
(32) Dahl, J. C.; Wang, X.; Huang, X.; Chan, E. M.; Alivisatos, A. P. Elucidating the Weakly Reversible Cs−Pb−Br Perovskite Nanocrystal Reaction Network with High-Throughput Maps and Transformations. *J. Am. Chem. Soc.* **2020**, *142*, 11915−11926.
(33) Imran, M.; Ijaz, P.; Goldoni, L.; Maggioni, D.; Petralanda, U.; Prato, M.; Almeida, G.; Infante, I.; Manna, L. Simultaneous Cationic and Anionic Ligand Exchange For Colloidally Stable $CsPbBr_3$ Nanocrystals. *ACS Energy Lett.* **2019**, *4*, 819−824.
(34) Pan, J.; Quan, L. N.; Zhao, Y.; Peng, W.; Murali, B.; Sarmah, S. P.; Yuan, M.; Sinatra, L.; Alyami, N. M.; Liu, J.; Yassitepe, E.; Yang, Z.; Voznyy, O.; Comin, R.; Hedhili, M. N.; Mohammed, O. F.; Lu, Z. H.; Kim, D. H.; Sargent, E. H.; Bakr, O. M. Highly Efficient Perovskite-Quantum-Dot Light-Emitting Diodes by Surface Engineering. *Adv. Mater.* **2016**, *28*, 8718−8725.
(35) Shynkarenko, Y.; Bodnarchuk, M. I.; Bernasconi, C.; Berezovska, Y.; Verteletskyi, V.; Ochsenbein, S. T.; Kovalenko, M. V. Direct Synthesis of Quaternary Alkylammonium-Capped Perovskite Nanocrystals for Efficient Blue and Green Light-Emitting Diodes. *ACS Energy Lett.* **2019**, *4*, 2703−2711.
(36) Park, J. H.; Lee, A.; Yu, J. C.; Nam, Y. S.; Choi, Y.; Park, J.; Song, M. H. Surface Ligand Engineering for Efficient Perovskite Nanocrystal-Based Light-Emitting Diodes. *ACS Appl. Mater. Interfaces* **2019**, *11*, 8428−8435.
(37) Moyen, E.; Jun, H.; Kim, H.-M.; Jang, J. Surface Engineering of Room Temperature-Grown Inorganic Perovskite Quantum Dots for Highly Efficient Inverted Light-Emitting Diodes. *ACS Appl. Mater. Interfaces* **2018**, *10*, 42647−42656.
(38) Abiodun, S. L.; Pellechia, P. J.; Greytak, A. B. Effective Purification of $CsPbBr_3$ Nanocrystals with High Quantum Yield and High Colloidal Stability via Gel Permeation Chromatography. *J. Phys. Chem. C* **2021**, *125*, 3463−3471.
(39) Smock, S. R.; Williams, T. J.; Brutchey, R. L. Quantifying the Thermodynamics of Ligand Binding to $CsPbBr_3$ Quantum Dots. *Angew. Chem., Int. Ed.* **2018**, *57*, 11711−11715.
(40) Grossoehme, N.; Spuches, A.; Wilcox, D. Application of Isothermal Titration Calorimetry in Bioinorganic Chemistry. *JBIC, J. Biol. Inorg. Chem.* **2010**, *15*, 1183−1191.
(41) Freyer, M. W.; Lewis, E. A. Isothermal Titration Calorimetry: Experimental Design, Data Analysis, and Probing Macromolecule/Ligand Binding and Kinetic Interactions. *Methods Cell Biol.* **2008**, *84*, 79−113.
(42) Moore, D. E.; Goode, D. R.; Seney, C. S.; Boatwright, J. M. Isothermal Titration Calorimetry Can Provide Critical Thinking Opportunities. *J. Chem. Educ.* **2016**, *93*, 304−310.
(43) Falconer, R. J. Applications of Isothermal Titration Calorimetry − the Research and Technical Developments from 2011 to 2015. *J. Mol. Recognit.* **2016**, *29*, 504−515.
(44) Archer, W. R.; Schulz, M. D. Isothermal Titration Calorimetry: Practical Approaches and Current Applications in Soft Matter. *Soft Matter* **2020**, *16*, 8760−8774.
(45) Shen, Y.; Tan, R.; Gee, M. Y.; Greytak, A. B. Quantum Yield Regeneration: Influence of Neutral Ligand Binding on Photophysical Properties in Colloidal Core/Shell Quantum Dots. *ACS Nano* **2015**, *9*, 3345−3359.
(46) Gee, M. Y.; Shen, Y.; Greytak, A. B. Isothermal Titration Calorimetry Resolves Sequential Ligand Exchange and Association Reactions in Treatment of Oleate-Capped CdSe Quantum Dots with Alkylphosphonic Acid. *J. Phys. Chem. C* **2020**, *124*, 23964−23975.
(47) Elimelech, O.; Aviv, O.; Oded, M.; Banin, U. A Tale of Tails: Thermodynamics of CdSe Nanocrystal Surface Ligand Exchange. *Nano Lett.* **2020**, *20*, 6396−6403.
(48) Jharimune, S.; Sathe, A. A.; Rioux, R. M. Thermochemical Measurements of Cation Exchange in CdSe Nanocrystals Using Isothermal Titration Calorimetry. *Nano Lett.* **2018**, *18*, 6795−6803.
(49) Calvin, J. J.; Swabeck, J. K.; Sedlak, A. B.; Kim, Y.; Jang, E.; Alivisatos, A. P. Thermodynamic Investigation of Increased Luminescence in Indium Phosphide Quantum Dots by Treatment with Metal Halide Salts. *J. Am. Chem. Soc.* **2020**, *142*, 18897−18906.
(50) Calvin, J. J.; O'Brien, E. A.; Sedlak, A. B.; Balan, A. D.; Alivisatos, A. P. Thermodynamics of Composition Dependent Ligand Exchange on the Surfaces of Colloidal Indium Phosphide Quantum Dots. *ACS Nano* **2021**, *15*, 1407−1420.
(51) Shen, Y.; Gee, M. Y.; Tan, R.; Pellechia, P. J.; Greytak, A. B. Purification of Quantum Dots by Gel Permeation Chromatography and the Effect of Excess Ligands on Shell Growth and Ligand Exchange. *Chem. Mater.* **2013**, *25*, 2838−2848.
(52) Protesescu, L.; Yakunin, S.; Bodnarchuk, M. I.; Krieg, F.; Caputo, R.; Hendon, C. H.; Yang, R. X.; Walsh, A.; Kovalenko, M. V. Nanocrystals of Cesium Lead Halide Perovskites ($CsPbX_3$, X = Cl, Br, and I): Novel Optoelectronic Materials Showing Bright Emission with Wide Color Gamut. *Nano Lett.* **2015**, *15*, 3692−3696.
(53) Almeida, G.; Goldoni, L.; Akkerman, Q.; Dang, Z.; Khan, A. H.; Marras, S.; Moreels, I.; Manna, L. Role of Acid−Base Equilibria in the Size, Shape, and Phase Control of Cesium Lead Bromide Nanocrystals. *ACS Nano* **2018**, *12*, 1704−1711.
(54) De Roo, J.; Ibáñez, M.; Geiregat, P.; Nedelcu, G.; Walravens, W.; Maes, J.; Martins, J. C.; Van Driessche, I.; Kovalenko, M. V.; Hens, Z. Highly Dynamic Ligand Binding and Light Absorption Coefficient of Cesium Lead Bromide Perovskite Nanocrystals. *ACS Nano* **2016**, *10*, 2071−2081.
(55) Grisorio, R.; Clemente, M. E. D.; Fanizza, E.; Allegretta, I.; Altamura, D.; Striccoli, M.; Terzano, R.; Giannini, C.; Irimia-Vladu, M.; et al. Exploring the Surface Chemistry of Cesium Lead Halide Perovskite Nanocrystals. *Nanoscale* **2019**, *11*, 986−999.
(56) Sandeep, K.; Gopika, K. Y.; Revathi, M. R. Role of Capped Oleyl Amine in the Moisture-Induced Structural Transformation of $CsPbBr_3$ Perovskite Nanocrystals. *Phys. Status Solidi RRL* **2019**, *13*, 1900387 DOI: 10.1002/pssr.201900387.
(57) Brautigam, C. A. Fitting Two- and Three-Site Binding Models to Isothermal Titration Calorimetric Data. *Methods* **2015**, *76*, 124−136.
(58) Chen, Y.; Smock, S. R.; Flintgruber, A. H.; Perras, F. A.; Brutchey, R. L.; Rossini, A. J. Surface Termination of $CsPbBr_3$ Perovskite Quantum Dots Determined by Solid-State NMR Spectroscopy. *J. Am. Chem. Soc.* **2020**, *142*, 6117−6127.
(59) Bodnarchuk, M. I.; Boehme, S. C.; ten Brinck, S.; Bernasconi, C.; Shynkarenko, Y.; Krieg, F.; Widmer, R.; Aeschlimann, B.; Günther, D.; Kovalenko, M. V.; Infante, I. Rationalizing and Controlling the Surface Structure and Electronic Passivation of Cesium Lead Halide Nanocrystals. *ACS Energy Lett.* **2019**, *4*, 63−74.
(60) Ijaz, P.; Imran, M.; Soares, M. M.; Tolentino, H. C. N.; Martín-García, B.; Giannini, C.; Moreels, I.; Manna, L.; Krahne, R. Composition-, Size-, and Surface Functionalization-Dependent Optical Properties of Lead Bromide Perovskite Nanocrystals. *J. Phys. Chem. Lett.* **2020**, *11*, 2079−2085.

https://doi.org/10.1021/acs.jpcc.1c00144
J. Phys. Chem. C 2021, 125, 17897−17905